Identification of the Sites of Chlorophyll Triplet Quenching in Relation to the Structure of LHC-II from Higher Plants. Evidence from EPR Spectroscopy

Marilena Di Valentin, Federico Biasibetti, Stefano Ceola, and Donatella Carbonera*

Dipartimento di Scienze Chimiche, Università di Padova, via Marzolo 1, 35131 Padova, Italy

Received: April 30, 2009; Revised Manuscript Received: July 24, 2009

The Chlorophyll a (Chl a) molecules involved in the triplet−triplet energy transfer to the central luteins in trimeric LHC-II are identified by time-resolved and pulse EPR techniques. The concept of spin angular momentum conservation during triplet−triplet energy transfer is exploited for the calculation of the spin polarization of the carotenoid triplet states. The sites with the highest probability of forming triplet states, which are quenched by the central luteins, result to be Chl603 and Chl612. "Unquenched" Chl triplet states are produced by photoexcitation in the LHC-II complex. Putative sites of these triplet states are Chl614, Chl611, Chl604, and Chl613 since they do not contribute to the formation of the observed carotenoid triplet states.

Introduction

In the photosystem II of higher plants, the main light harvesting function is played by the LHC-II Chl a/b-binding complex, which is the most abundant membrane protein in the chloroplasts. The crystal structure of the spinach LHC-II complex has been obtained to a resolution of 2.72 Å[1] and that of pea to a resolution of 2.5 Å.[2] The folding of the LHC-II protein is characterized by three trans-membrane helices, and a trimer assembly has been observed. The high-quality electron density map permitted the location of all 14 chlorophylls (Chls), eight Chl a and six Chl b, within one monomeric unit of the LHC-II complex. Three carotenoids (Cars) were also clearly identified as corresponding to two luteins and one neoxanthin. One site of mixed density was assigned to the carotenoids involved in the xanthophyll-cycle (namely, violaxanthin, antheraxanthin, zeaxanthin), which play an important role in the nonradiative dissipation of excess excitation energy formed under high light conditions.[3] Luteins are bound in the center of the protein in sites L1 and L2 (see Figure 1). The binding site N1 is specific for neoxanthin and is located near the helix C. The V1 site may bind violaxanthin, lutein, or zeaxanthin depending on light conditions[4] and is located at the periphery of the monomeric subunits.

In high light conditions, the radiation absorbed by the light harvesting system can not be completely processed by the electron transport chain, and dissipation via other mechanisms becomes essential to avoid damage. The main photoprotective mechanism responsible for the excess energy dissipation in LHC-II is catalyzed by the nonphotochemical quenching (NPQ) mechanism based on the de-epoxidation of violaxanthin to antheraxanthin and zeaxanthin (VAZ) by violaxanthin de-epoxidase, which is activated by low luminal pH[3] and probably involves the V1 site.[4] Carotenoids in V1 are not involved in light-harvesting and singlet energy transfer.[5]

Quenching in LHC-II or in the minor light-harvesting complexes is widely assumed to be caused by a conformational change that switches the complex from the active, energy-transmitting state to a quenched and dissipative state.[6−9] It has been suggested that L1 can be a site of fast response to the qE, the energy dependent quenching component of NPQ:[6,7] this site seems to undergo a conformational change as a consequence of a neoxanthin-triggered mechanism leading to the formation of a lutein−Chl a heterodimer capable of dissipating the excitation energy via a carotenoid excited singlet state. This proposed mechanism would seem to involve, in vivo, an aggregation-induced conformational change of the LHC-II proteins. However, this interpretation is still under debate in the literature. Recently, Barros et al. observed a strong emission and comparatively long fluorescence lifetime in single LHC-II crystals, indicating that the complex is unquenched and thus that the crystal structure shows the active, energy-transmitting state of LHC-II.[10] Starting from this observation, they came to the conclusion that excitation energy quenching, in the light-harvesting complexes, is due to the molecular interaction with external pigments in vitro or other pigment−protein complexes such as PsbS in vivo and does not require a conformational change within the complex. Thus, at present, there is no conclusive evidence of a conformational change of LHC-II.

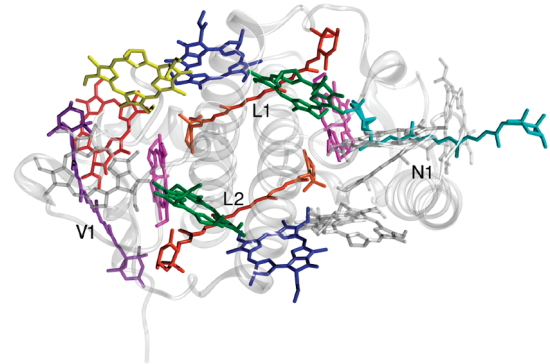

Figure 1. Structure of the pigments associated with the basic unit of the LHC-II complex.[1] Structure derived from coordinates deposited in the Brookhaven Protein Data Bank (1 RWT). The protein backbone and the Chl b molecules are in faded gray. Orange, luteins in site L1 and L2; purple, violoxanthin (Xat) in site V1; cyan, neoxanthin (Nex) in site N1; blue, Chl a603 (lower) and 612 (upper); pink, Chl a604 (right) and 613 (left); green, Chl a602 (left) and 610 (right); yellow, Chl a611; red, Chl a614.

* Author to whom correspondence should be addressed. Tel.: +39 498275144. Fax: +39 498275161. E-mail: donatella.carbonera@unipd.it.

10.1021/jp904012j CCC: $40.75
Published on Web 09/03/2009

An alternative mechanism for the qE quenching based on the formation of a Zeaxanthin radical cation and a Chl radical anion has also been proposed.[11] However, the involvement of a zeaxanthin−Chl charge separated state in the dissipation of high excitation density seems to be a specific characteristic of the minor antenna complexes, while LHC-II, at least in vitro, does not show the presence of the Car cation formation up to the femtosecond time scale.[12]

Carotenoids in LHC-II are also known to be involved in the photoprotection process as efficient, fast, and direct quenchers of the Chl triplet states, thus preventing the formation of singlet oxygen ($^1O_2$*) and subsequent harmful oxidation of membrane and protein elements.[13] This is the fastest response to the requirement of energy dissipation in the complex. The study of Car triplet states formed in LHC-II complexes has been performed in the past by means of different spectroscopic techniques (EPR, ODMR, time-resolved optical spectroscopy).[14−22] Different Car triplet states have been characterized, showing specific interactions with nearby Chl molecules.[16] Lampoura et al.[20] assigned the Car triplets specifically to the luteins in sites L1 and L2, excluding the violaxanthin in the V1 site, since this carotenoid is not involved in singlet energy transfer and therefore cannot be involved in triplet quenching, which is a mechanism requiring closer vicinity between the donor and the acceptor. In addition, neoxanthin was excluded from participating in triplet quenching on the basis of its being surrounded by Chl b molecules which transfer the excitation to Chl a molecules so quickly that the probability of populating Chl b triplet states should be negligible. However, the recently published structures of LHC-II at high resolution[1,2] have shown that both neoxanthin and violaxanthin are close to at least one Chl a molecule, thus, in principle, their involvement in triplet quenching cannot be excluded.

Starting from the most recent crystallographic data, Mozzo et al.[23] re-examined the problem of the carotenoid triplet assignment. They used laser-induced Triplet-minus-Singlet (TmS) spectroscopy on LHC-II preparations with different carotenoid composition and came to the conclusion that the largest part of the triplets is quenched by the lutein bound in site L1, in close proximity to the low-energy chlorophylls of the complex. The lutein in the L2 site is also active in triplet quenching, showing a longer triplet lifetime. To study the triplet quenching contribution of the carotenoids in the V1 and N1 sites, the TmS spectra of LHC-II with an empty V1 site and of LHC-II lacking both neoxanthin and violaxanthin were measured by the authors and compared with those of the wild type (WT). The shape of the spectra and the relative amplitudes of the components were only slightly different in the two complexes compared to the WT, indicating that the carotenoids in the V1 and N1 sites do not participate in triplet quenching. However, the spectral lines were too broad to exclude the presence of extra contributions with certainty, and the measurements were not accompanied by an estimate of the triplet yield in the two different samples. Moreover, small differences in the lifetimes of the spectral components were observed, in the above-mentioned LHC-II complexes. Thus, although Mozzo et al.[23] assigned the observed triplet states to the carotenoids present in the structure, further investigation is needed especially to identify the Chl molecules where the triplet states are initially formed and to exclude the involvement of the N1 and V1 sites.

In the past, we used ODMR (optically detected magnetic resonance) to study the formation of triplet states in isolated LHC-II complexes, showing the presence of at least two distinct populations of carotenoid triplet states.[16,17] More recently, in a time-resolved electron paramagnetic resonance (TR-EPR) and pulse-EPR work on the peridinin triplet state generated in PCP proteins from *Amphidinium carterae*, we exploited the concept of spin conservation during triplet−triplet energy transfer (TTET) to identify the peridinin−chlorophyll pairs directly involved in the process.[24,25]

In this work, we apply the advanced EPR techniques to get insight into the mechanism of formation of the carotenoid triplet states in LHC-II. We take advantage of the analysis approach previously used for PCP to identify the sites of the Chl triplet formation and quenching by carotenoids, in relation to the protein structure of LHC-II in higher plants.

The EPR data are discussed in terms of energy transfer properties, specific pathways for triplet quenching, and protein structure.

Materials and Methods

Sample Preparation. The LHC-II complexes were isolated from spinach by using *n*-octyl-β-D-glucopyranoside[26] after which the LHC-II trimers were purified by using *n*-dodecyl-β-D-maltoside and were ultracentrifuged. For measurements, the samples were diluted in 10 mM Tricine, pH 7.8, 0.3 M sucrose, and 0.03% w/v β-dodecylmaltoside, to a final protein concentration of 3 mg/mL.

Oxygen was removed from the samples by flushing argon in the EPR capillary before freezing. Glycerol, previously degassed by several cycles of freezing and pumping, was added (60% v/v) to obtain a transparent matrix.

TR-EPR. TR-EPR spectra were obtained in direct detection mode using pulsed light excitation. The X-band EPR spectrometer (Bruker ECS106) was equipped with a TE102 cavity (9.4 GHz) and a nitrogen flow system. For measurements at cryogenic temperatures, an Oxford helium cryostat (ESR 200) was used. Laser excitation at 532 nm (10 mJ per pulse and repetition rate of 10 Hz) was provided by the second harmonic of a Nd:YAG laser (Quantel Brilliant). The time resolution of the TR-EPR spectrometer is about 150 ns. The microwave power used for the TR-EPR experiments was 20 mW at the cavity. No field modulation or phase-sensitive detection was used. The EPR signals were taken from the microwave preamplifier (ER047-PH Bruker, bandwidth 20 Hz−6.5 MHz) and sampled with a LeCroy LT364 oscilloscope (1 ns per point). To eliminate the laser background signal, transients were accumulated under off-resonance field conditions and subtracted from those on-resonance. The spectra at different times after the laser pulses were reconstructed from kinetic traces for each field position.

Pulse EPR Experiments. Experiments were performed on a Bruker Elexsys E580 pulsed EPR spectrometer. Laser excitation at 532 nm (10 mJ per pulse and repetition rate of 10 Hz) was provided by the second harmonic of a Nd:YAG laser (Quantel Brilliant) in a dielectric cavity. The temperature was controlled by means of a Helium cryostat (Oxford CF935) driven by a temperature controller (Oxford ITC503).

Field-swept electron spin echo (ESE) spectra (FSE spectra) were recorded using a two-pulse ESE sequence according to the scheme: flash-DAF-π/2-τ-π-τ-echo (DAF = delay after laser flash); the value of DAF was fixed at 50 ns, which was, in our setup, the shortest time for the detection which follows the trigger after the laser pulse. ESE-detected kinetics at the triplet canonical orientations were recorded using a two-pulse (flash-DAF-π/2-τ-π-τ-echo) ESE sequence after a variable DAF between the laser flash and the first MW pulse. The π/2-pulse was of 16 ns, and the delay τ was set at 200 ns for the FSE experiment and to 120 ns for the ESE-detected kinetics.

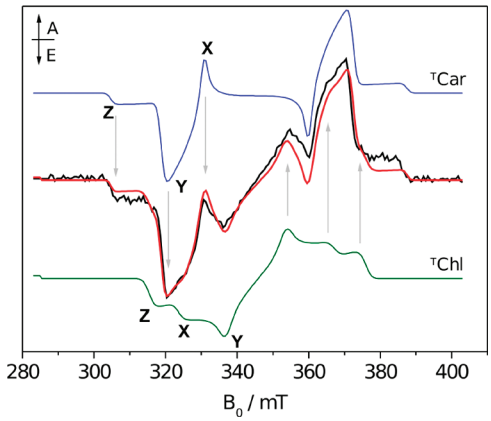

Figure 2. TR-EPR spectrum of LHC-II (black line) taken 150 ns after the laser pulse at 20 K. *X*, *Y*, *Z* represent the ZFS canonical orientations. Reconstruction of the LHCII TR-EPR spectrum (red line), deriving from ^{3}Car (blue line) and ^{3}Chl a (green line) contributions, in proportion, respectively, 1:0.3. Parameters for the reconstruction are reported in Table 1. *A* = absorption, *E* = emission.

EPR Spectral Analysis. Calculation of the sublevel triplet state populations of the acceptor, starting from those of the donor, was performed using a home-written program in MatLab software, following the formalism of refs 24 and 27 and utilizing the X-ray coordinates of the pigment moieties. The carotenoid zero filed splitting (ZFS) axes were determined therein using principal components analysis. The method is based upon the solution of the covariance matrix of the data, in which the eigenvalues represent the amount of variance explained by each eigenvector. The data set used in the calculations contained simply the three spatial coordinates of the atoms of each Car (only those of the conjugated chain), as reported in the PDB file 1RWT, resulting therefore in the eigenvectors being a good approximation of the ZFS axes. This is due to the particular orientation of the Car's ZFS axes: the first solution vector is the one with the greatest eigenvalue (which explains most of the variance) and thus lies along the main axis (*Z*) of the Car. The second one has the second biggest eigenvalue and thus lies along the C−H bonds (*X*). The third vector is orthogonal to the first two (*Y*). The calculation was made using the MatLab function named "princomp". The program works in the limit of a TTET which is fast, compared to the time evolution of the donor triplet spectrum, and is slow enough to allow spin alignment in the external magnetic field.

Simulations of the powder spin-polarized triplet spectra were performed using a program written in MatLab with the aid of the Easyspin routine (ver. 2.6.0).[28] The program is based on the full diagonalization of the triplet state spin Hamiltonian, taking into account the Zeeman and magnetic dipole−dipole interactions, assuming a powder-like distribution of molecular orientations with respect to the magnetic field direction. Input parameters are: the sublevel populations, the ZFS parameters, the line width at the canonical orientations, and the g-tensor components.

Results

Figure 2 shows the X-band spin-polarized TR-EPR spectrum of LHC-II, taken at 150 ns after the laser pulse, at 20 K. The spectrum reveals the presence of different species. The prevalent triplet population, having ZFS parameters, $|D| = 414$ G and $|E| = 40.7$ G, can be easily assigned to the carotenoid species, ^{3}Car, on the basis of the comparison with the previously reported values of the ZFS parameters determined by ODMR spectroscopy.[16,17] The other species can be assigned to the Chl a triplet state (^{3}Chl a) on the basis of the ZFS parameters,[24,29] as can be clearly seen by comparison with the spectrum of ^{3}Chl a reported in the same figure. This spectrum has been obtained by simulation of the TR-EPR of ^{3}Chl a in micelles of Triton X-100 1 mM, detected under the same experimental conditions as for LHC-II (see Supporting Information). Because of the large spectral overlap of the two triplet states, it is not easy to determine the exact polarization patterns of the two contributing triplet states by direct inspection of the TR-EPR spectrum. For this reason, we also performed pulse-ESE experiments, on the same sample, to try to better discern the different components.

ESE spectroscopy is based on the principle of spin refocusing after a microwave pulse sequence. We have previously demonstrated that the TR-EPR and FSE spectra, taken at short delay after the laser flash (DAF), were identical for the PCP samples, where only carotenoid triplet states were present,[30] due to the absence of fast and anisotropic relaxation processes which depend on the orientation of the carotenoid triplet states in relation to the magnetic field. On the contrary, porphyrin triplet states are known to show anisotropic relaxation processes which are reflected in their FSE spectra.[31] In Figure 3, we report the FSE spectrum of LHC-II, at DAF = 50 ns. Direct comparison of the FSE and TR-EPR spectra reveals that the central lines attributed to the *Y* component of the ^{3}Chl are almost suppressed in the FSE spectrum, leaving the contribution of the carotenoid easily discernible. A small contribution at the *Z* and *X* canonical orientations of ^{3}Chl to the FSE spectrum is however still visible. In Figure 3, we report also the FSE spectrum of ^{3}Chl dissolved in Triton X-100 (1 mM), detected at the same τ and DAF used for LHC-II. It can be seen that the shape of the FSE spectrum of ^{3}Chl is quite different compared to the corresponding TR-EPR, shown in Figure 2 (see also Supporting Information). By subtracting a proper amount of the experimental ^{3}Chl a FSE spectrum from the LHC-II spectrum, the "pure" contribution of ^{3}Car is obtained (Figure 3).

In this way, the correct polarization pattern of the ^{3}Car, *eeaeaa*, appears. As stated before, the FSE spectrum of the ^{3}Car is expected to be identical to the corresponding TR-EPR spectrum, while in the case of ^{3}Chl they differ significantly. We have therefore reconstructed the TR-EPR spectrum of LHC-II, using a simulation of the FSE-spectrum of ^{3}Car and a simulation of the TR-EPR spectrum of ^{3}Chl obtained in micelles of Triton X-100. These two pure contributions are shown in Figure 2. A good agreement with the experimental TR-EPR spectrum of LHC-II is reached, with the relative contributions reported in Table 1. Thus, despite the large spectral overlap of the ^{3}Chl and ^{3}Car, the simultaneous reconstruction of the TR-EPR and FSE spectra allows us to determine the spin polarization of the ^{3}Car with accuracy. This is an important starting point for further analysis.

Note that a contribution from a radical species is also present in the central part of the FSE spectra. This contribution has been neglected in the reconstruction of the spectra.

The kinetics of population and decay of the carotenoid triplet spin sublevels, obtained by monitoring the echo intensity as a function of DAF at the low-field canonical orientations of the ZFS tensor of the carotenoid triplet state (*Z*, *Y*, *X*, indicated in Figure 2), are shown in Figure 4. Inversion of the spin polarization at long delay times is expected on the basis of the anisotropy of the decay rates of the spin sublevels reported previously for other carotenoid triplet states.[15,30,32] The presence of the ^{3}Chl contribution affects the kinetics during the first few microseconds especially in the *X* canonical direction of the ^{3}Car,

TABLE 1: Simulation Parameters for the Triplets in the Reconstruction of the TR-EPR Spectrum of LHC-II[a]

	$\|D\|$	$\|E\|$		Wx:Wy:Wz	
	Gauss	Gauss	Px:Py:Pz	Gauss	relative contribution
carotenoid	414 ± 0.5	40.7 ± 0.5	0.40:0.20:0.40	15 ± 1:20 ± 1:20 ± 1	1
Chl a	310.3 ± 0.5	43.5 ± 0.5	0.36:0.44:0.20	25 ± 1:25 ± 1:25 ± 1	0.3

[a] Px,Py,Pz: zero-field populations of the triplet states; $|D|$, $|E|$: ZFS parameters; W = line-width at the canonical positions in the EPR powder spectrum. Frequency of the spectrometer: ν = 9.70 GHz. Isotropic g value: g_{iso} = 2.0023.

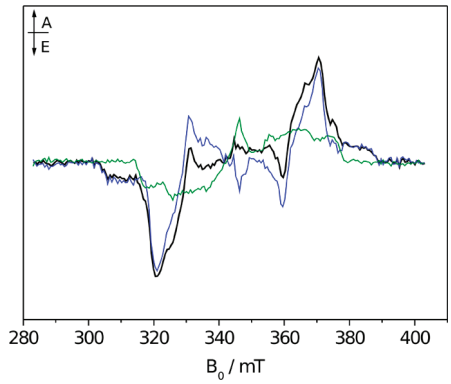

Figure 3. FSE spectrum of LHC-II (black line) and of ^{T}Chl a in micelles of Triton X100 (green line). Pure contribution of the carotenoid triplet state (blue line) to the field-swept ESE spectrum obtained after subtraction of the ^{T}Chl a spectrum in the proportion indicated by the green spectrum. A = absorption, E = emission.

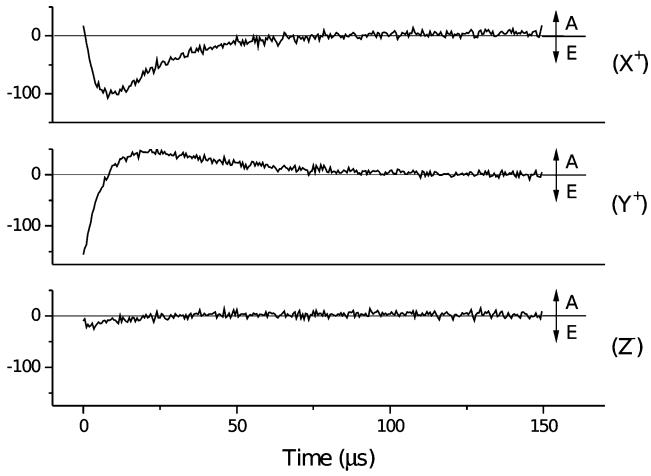

Figure 4. ESE-detected kinetics, at T = 20 K, at the low-field canonical fields Z^-, Y^+, X^+ of ^{T}Car indicated in Figure 2. A = absorption, E = emission. For other experimental conditions, see the Materials and Methods.

while in the Z and Y directions, the ^{T}Chl contribution is negligible. The kinetics show that the time evolution of the polarization is slow compared to the time resolution of the experiments.

Calculation of the Spin Polarization of the Carotenoid Triplet State Based on Spin Conservation during Triplet−Triplet Energy Transfer. The carotenoid triplet state formation in LHC-II occurs in the nanosecond time scale,[7] and it is thought to arise from ^{T}Chl quenching since the direct population starting from excited singlet states, by Inter System Crossing, is a very low probability process for carotenoids. The time resolution of our TR-EPR setup is about 150 ns, while the FSE spectrum was taken at 50 ns after the laser flash. This means that, in both cases, in the hypothesis of TTET between Chl and Car, we are able to detect only the acceptor triplet state, which is the ^{T}Car. The time evolution of the EPR signal of the acceptor is slow, 3 to 40 μs depending on the zero field principal axis direction, compared to its formation so that we can consider the first detected spectra as the "initial" spin polarized spectra, maintaining the polarization inherited from the ^{T}Chl donor.

The ^{T}Chl contribution to the LHC-II spectrum belongs to a Chl population which is unprotected and is not able to transfer the triplet energy to the carotenoids. In fact, there is no correlation between the decay rate of the observed ^{T}Chl and the ^{T}Car risetime.

As we have stated before, our aim is to analyze the carotenoid acceptor triplet state polarization in terms of the TTET mechanism from the ^{T}Chl a donor, by exploiting the principle of spin conservation during TTET. The fast transfer time allows us to state that the initial polarization pattern of ^{T}Chl a does not evolve significantly under the effect of spin relaxation before being transferred to the carotenoid. Since we are not able to detect the spectrum of the ^{T}Chl a donor directly, the transfer being too fast compared to the time resolution of the setup, we have to make some assumptions in terms of ^{T}Chl a sublevel populations, to be used for the calculation of the acceptor triplet populations. In the literature there are mainly two different sets of Chl triplet populations which have been reported from in vitro studies, depending on the polarity of the solvent and on the ligation state of the central Mg.[24,33,34] The ^{T}Chl a spectra, calculated starting from these two sets of populations, differ from each other in the initial polarization pattern (*eeeaaa* vs *eaeaea*). In the experiments performed on LHC-II, the ^{T}Chl a population which is not quenched by the carotenoid and is visible in the EPR spectrum has the polarization pattern *eeeaaa* (see Figure 2). In the following, we present the calculations for the acceptor populating rates obtained starting from the ^{T}Chl a spin populations which produce this spectral pattern, although, as the calculations demonstrate, the choice between the two polarization patterns does not influence the main conclusions that can be drawn from the results (Supporting Information).

The other parameters of the calculations are the directions of the ZFS axes, in relation to the molecular frame of each of the two partners, and the relative position in space of the donor and the acceptor moieties. The ^{T}Chl a ZFS axes have been chosen according to literature data[35,36] and are shown in Figure 5. The ZFS axes of the carotenoid triplet state have been chosen analogously to those determined for β-carotene in crystals.[37] The Z axis is along the polyene chain; the X axis is along the C−H bonds in the conjugated chain; and the Y direction is perpendicular to the conjugated XZ molecular plane (see Figure 5). Since the carotenoids in LHC-II are slightly distorted in the X-ray structure, we used a principal component analysis to derive the actual ZFS axes directions, as described in the Materials and Methods. An example of the resulting ZFS axes is shown for Lut620 in Figure 5C.

Under these assumptions, we calculated the carotenoid triplet spectra for all the Chl a−Car mutual configurations reported in the X-ray structure of LHC-II. In spite of the pseudo C_2 symmetry relating the two subclusters of pigments in the protein complex, differences are present in the relative position of the

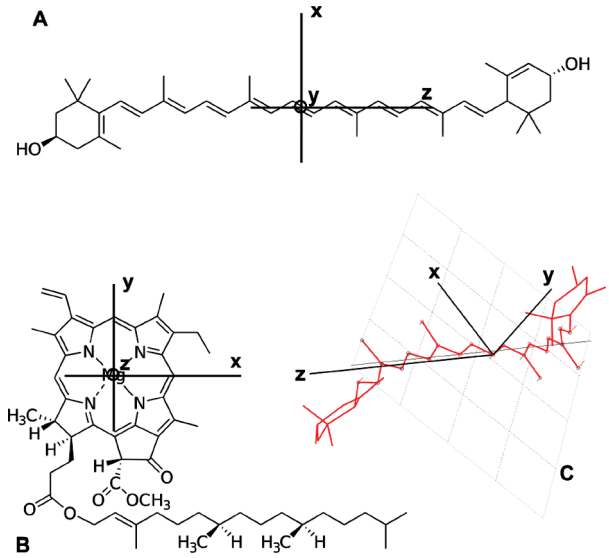

Figure 5. Scheme of the molecular structures of lutein (A) and chlorophyll a (B), with the orientation of the ZFS tensor axes. Orientation of the ZFS axes determined for Lut620 (C) calculated with the method described in the Materials and Methods section.

TABLE 2: Shortest Distances (in Å) between the π Systems of the Four Carotenoids and the Chl Molecules of LHC-II Complex

	Lut620	Lut621	Xat622	Nex623
Chl a				
602		3.41		
603		3.70		
604	8.59	4.10		4.21
610	3.61			
611	9.27		7.74	
612	3.65			
613	3.88	9.81	6.71	
614	7.31		7.28	
Chl b				
601		9.14	4.40	
605				
606		5.91		3.90
607		5.27	4.91[a]	
608				4.70
609		8.06		8.20

[a] Chl b from adjacent monomer.

homologous Chl−Car couples and in the local distortions of the carotenoid molecules, which must be considered in the calculations.

The shortest distances between the π-systems of the four carotenoids of the LHC-II monomer, namely, Lut620, Lut621, Xat622, and Nex623 (numbering from the 1RWT file[1]), and the Chl molecules are reported in Table 2. Car−Chl couples having distances >8 Å are not taken into account in our calculations since TTET, being based on the Dexter mechanism, requires close vicinity of the donor−acceptor pair. For this reason, intermonomer TTET is also excluded. Although Chl a and Chl b molecules are both reported in the table, only Chls a are considered for the calculation of the TTET because the fast singlet energy transfer from Chl b to Chl a makes the possibility of forming triplet states starting from Chl b singlet states negligible.

In Figure 6, the polarized triplet spectra calculated for Lut620 and Lut621, starting from each of the Chl a molecules located at a distance <8 Å, are reported and compared to the carotenoid contribution to the experimental FSE spectrum. The latter,

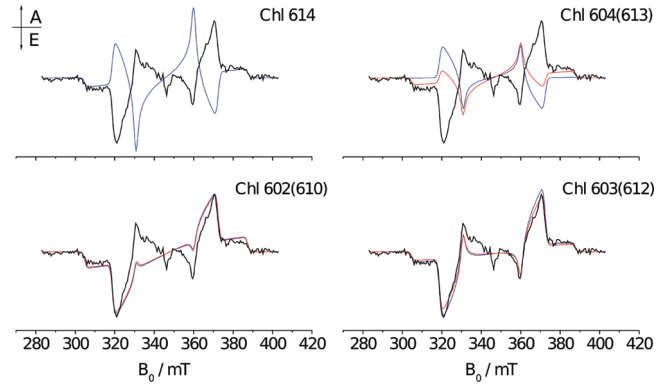

Figure 6. Calculated spin polarized triplet spectra for Lut620 (blue lines) and Lut621 (red lines) as populated by TTET from all the Chl a molecules located at a distance <8 Å, as indicated. Parameters of the calculations are reported in Table 3. Each calculated spectrum is compared to the carotenoid component of the experimental FSE spectrum reported in Figure 3.

showing the initial polarization of the ^{T}Car populated in LHC-II, is derived after subtracting the Chl triplet contribution (see Figure 3). The parameters for the calculation are reported in Table 3. It can be easily seen that the best agreement with the experiments is reached considering TTET from Chl a 603 and 612 to Lut621 and Lut620, respectively.

The results for the TTET from Chl611, 613, 614 to violaxanthin (Xat622) are shown in Figure 7. Only the transfer from Chl613 gives a polarization for ^{T}Xat622 which is compatible with the experimental spin polarization pattern *eeaeaa* (the parameters are reported in Table 3).

It must be noted that we used the same ZFS parameters as for the lutein triplet state calculations since there is not evidence, in the spectrum, of the presence of carotenoid triplet contributions characterized by different ZFS parameters.

Finally, the TTET from Chl 604 to neoxanthin (Nex623) is also considered. The spectrum, calculated with the parameters reported in Table 3, is shown in Figure 7. Again, we used the same ZFS parameters used for Lutein and Violaxanthin. However, it is worth noting that, since neoxanthin is present in a 9-cis conformation, a significant change of ZFS parameters should be expected. Moreover, the ZFS axes directions cannot be easily defined being that the cylindrical symmetry is lost. For this reason, the calculations have been performed also exploring a rotation of ±45° around the *Y* axis defined as perpendicular to the conjugated π plane. In all the explored directions of the ZFS axes, the agreement with the experimental spectrum is poor (not shown).

A similar approach has also been used to test the robustness of the results for each of the Car−Chl couples examined. A rotation of the Car ZFS axes around each of those initially determined by the principal component analysis has been performed, and the changes of the spectra produced by the rotations have been examined. The calculations indicate that all the results remain valid for rotations up to, at least, ±15°, except for the couple Chl a602(610)−Lut621(620) for which the polarization of the acceptor ^{T}Car changes dramatically upon rotation around the *Y* and *Z* axes. In this case, it is possible, only for few and specific rotation patterns, to obtain spectra which are in agreement with the experimental one (Supporting Information).

Discussion

From the calculations reported in the previous section, it is clear that the initial polarization of the ^{T}Car component in the

TABLE 3: Parameters of Carotenoid Triplet State Simulations[a]

	subcluster Lut 621			subcluster Lut 620				Xat622			Nex623
	Chl602	Chl603	Chl604	Chl610	Chl612	Chl613	Chl614	Chl611	Chl613	Chl614	Chl604
Px	0.35	0.41	0.26	0.35	0.41	0.30	0.23	0.21	0.38	0.42	0.34
Py	0.29	0.22	0.37	0.28	0.21	0.37	0.41	0.41	0.24	0.37	0.43
Pz	0.36	0.37	0.37	0.37	0.38	0.33	0.36	0.38	0.38	0.21	0.23
	$\|D\| = 414 \pm 0.5$ G ($387.0 \pm 1.4 \times 10^{-4}$ cm^{-1})										
	$\|E\| = 40.7 \pm 0.5$ G ($38.0 \pm 0.5 \times 10^{-4}$ cm^{-1})										
	$Wx = 15 \pm 1$ G										
	$Wy = 20 \pm 1$ G										
	$Wz = 20 \pm 1$ G										

[a] *Px*,*Py*,*Pz*, population of the triplet state sublevels of each carotenoid present in LHC-II, calculated on the basis of the spin conservation during TTET starting from the ^{T}Chl a sublevel populations. *Px*:*Py*:*Pz* = 0.36:0.44:0.20. $|D|$, $|E|$ = ZFS parameters (the same values are used for the three different carotenoids); *W* = the line-width at the canonical positions in the EPR powder spectrum. Frequency of the spectrometer: ν = 9.70 GHz. Isotropic *g* value: $g_{iso} = 2.0023$.

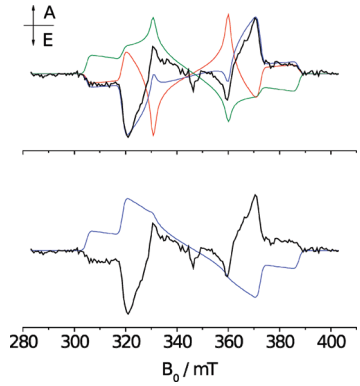

Figure 7. Top: spin polarized triplet spectra calculated for Xat622 as populated by TTET from all the Chl a molecules located at a distance <8 Å. Red line: Chl611; Blue line: Chl613; Green line: Chl614. Bottom: spin polarized triplet spectrum calculated for Nex623 starting from Chl604. Each calculated spectrum is compared to the carotenoid component of the experimental FSE spectrum reported in Figure 3.

LHC-II EPR spectrum can be reproduced by invoking a TTET mechanism in which the triplet that initially forms in specific Chl molecules in the complex is finally transferred to the carotenoids. The studies performed in the past on natural and synthetic systems have shown that the advanced EPR techniques represent powerful tools for investigating the triplet formation mechanisms.[15,24,25,32,33,38] One of the currently open questions on the comprehension of the photophysical behavior of the light harvesting complexes of higher plants is whether and when charge separated states may be invoked to explain the qE dissipation mechanism. The observed spin polarization pattern of the ^{T}Car, *eeaeaa*, rules out the possibility that the carotenoid triplet state, in LHC-II trimers in the "unquenched state", is populated as a result of a charge recombination from a charge separated state [Car^{+}Chl^{-}] with a singlet precursor. In this case, the expected polarization pattern would be *eaaeea*.[38] Since TTET has even more stringent distance requirements than electron transfer,[39,40] it is likely that in the light-harvesting complexes, at least in the "unquenched state", the electron transfer process, and the consequent energy loss, is avoided by selecting a nonpolar environment of the Car−Chl couples,[41] thus making the charge transfer state formation less favorable compared to TTET. Studies on synthetic caroteno−pheophorbide dyads in vitro have shown that it is possible to switch from a charge separation to a TTET mechanism by substitution of a polar solvent with a nonpolar one.[42] Thus, it is very unlikely that the central luteins which are active in the TTET in the "unquenched" state of LHC-II could be transformed into sites of charge transfer and energy dissipation in the "quenched" state, by a conformational change which leads to a shortening of the Car−Chl distances,[9] without a change in the polarity of the medium.

In the TTET mechanism, the relative geometry of the donor−acceptor pair is of fundamental importance. In the LHC-II complex, the presence of four carotenoids surrounding several Chl a molecules, at comparable short distances, makes the question regarding the most favorable pathway of triplet quenching by no means trivial.

The spectral analysis reported in the Results section has shown that the initial polarization of the triplet state detected in LHC-II may be reproduced by considering a single TTET step from Chl603 to Lut621 and/or from Chl612 to Lut620. It is worth noting that this result does not depend critically on the assumptions which have been adopted to perform the calculations. The model of energy transfer in LHC-II by Novoderezekin et al. suggested that the red-most chlorophylls in the two lutein domains are, respectively, Chl602 and Chl610.[43] In principle, it can be expected that these sites should be the most likely to develop triplet states. The possibility that the transfer from Chl602/Chl610 to the two central luteins may contribute to the detected TTET can not be ruled out on the basis of our results since the calculated polarization is characterized by a spin polarization pattern, *eeaeaa*, similar to the experimental one. However, the agreement with the experiments is not as satisfactory as for the couple Chl603/612 and is very much dependent on both the choice of the ZFS axes directions and the ^{T}Chl a spin sublevel populations (Supporting Information). A further analysis showed that also a two-step TTET involving Chl 610, i.d. Chl610 (603) → Chl 612 (602) → Car and Chl612 → Chl 610 → Car, does not produce the correct polarization for the acceptor carotenoid triplet state (not shown). This excludes the possibility that the red-most Chl a molecules might transfer the triplet energy to the nearby Chls, through an activated TTET, before the carotenoid quenching takes place.

Until recently, LHC-II was considered to be in a quenched state in crystals.[2,9] It was also suggested that the quenched state could be accompanied in vivo by a conformational change of the complex, leading to the nonphotochemical quenching, qE. Ruban et al.[7] suggested that this conformational change may interest the site of Lut620 bringing it closer to Chl612. This would produce a dissipative state, the one observed in the X-ray structure, because, in this way, Chl excitation could be quickly transferred to a low lying carotenoid excited state.[7] Studies on phthalocynine−carotenoid dyads showed that the carotenoid S_1−ICT (intramolecular charge transfer) state may become lower in energy compared to the Q_y state of Chl, acting as an energy dissipating state, depending on the carotenoid length, backbone conformation, and polarity of the solvent.[41] However,

more recently, Barros et al.[10] demonstrated that the structures of pea and spinach LHC-II are identical within experimental error and concluded that the striking disappearance of the 680 nm fluorescence peak cannot be taken as a proof that the crystal structure shows a quenched state of the complex. Thus, we are confident that our calculations based on the pigment coordinates of the X-ray structure are meaningful for LHC-II in solution and in an "unquenched" state.

In the crystal structure, the two central luteins have slightly different conformations.[6] Our calculations demonstrate that these conformational differences produce minor effects in terms of the expected polarization of the carotenoid triplet spectrum, showing that both Chl603 and Chl612 can be sites of triplet formation. We also repeated the analysis starting from the X-ray coordinates reported for the crystals of pea LHC-II.[2] As expected, the differences present in the two crystals produce only minor effects on the calculated spectra (not shown) and do not alter the conclusions about the triplet quenching sites.

The calculations prove that Chl613, 604, 614, and 611 cannot be sites where triplet states are formed and subsequently quenched by luteins since they do not contribute, with a significant weight, to produce the spin polarization pattern of the observed ^{T}Car.

Although the results coming from optical spectroscopy experiments seem to suggest that Violaxanthin, in the V1 site, and Neoxanthin, in the N1 site, are likely not involved in TTET from chlorophyll triplet states, we have tried to provide an independent demonstration for this conclusion through EPR spectroscopy. We found that, while any role of neoxanthin is ruled out because there is no calculated spectrum of the triplet state of this carotenoid which is in agreement with the experimental one, TTET from Chl613 to violoxanthin gives a polarization pattern which is compatible with the observed triplet spectrum. Although the shortest distance between these two pigments, of 6.71 Å, makes the transfer very unlikely, it cannot be excluded on the basis of the EPR results.

As reported previously,[23] the chlorophyll to carotenoid TTET is efficient but not complete, leaving about 5% of the chlorophyll triplets unquenched. These "unprotected" chlorophylls were proposed to belong mainly to a Chl a population sitting in the Chl611 site.[23] On the basis of our results, possible sites of "unquenched" triplet states are Chl614, Chl611, Chl604, and probably also Chl613. They do not contribute to the formation of the observed carotenoid triplet states, and thus if their triplet states become populated, they cannot be quenched by carotenoids. Previously reported TmS spectra, at low temperature, associated with the Chl millisecond components of the triplet state in LHC-II, show a broad bleaching at wavelengths between 670 and 680 nm,[19] indicating that more than one Chl site is involved in the formation of unquenched triplet states. The Chl triplet states observed in LHC-II may in principle be formed in Chls which are not connected, via singlet−singlet energy transfer, to the functional network of pigments. This could be an artifact due to the low temperatures of the EPR experiments because of the freezing procedure which may introduce some heterogeneity in the pigment organization. However, Croce et al.[28] showed that unquenched Chl triplet states were formed in isolated LHC-II even at room temperature and proved that the antenna pigments were thermally equilibrated, leading to the conclusion that the Chl triplet states were not due to disconnected Chl molecules. Therefore, we think that also the Chl triplet formation observed at low temperature, with its specific thermal distribution of the excitation, is due to the molecular structure of LHC-II. Site energy of the Chl molecules, singlet−singlet energy transfer efficiency, and exciton interactions among the pigments are all important elements in determining the specific sites with a higher triplet formation probability. The role of these Chl triplet states in the damage of the system under physiological conditions may be not relevant if in the intact photosystem the Chls giving the triplet states are peripheral and can transfer their singlet excitation to nearby complexes. Moreover, it is known that under light-stress conditions the NPQ process prevents the damage of the photosystem by acting at the level of the excited singlet states thus making the formation of Chl triplet states unlike.

Conclusions

We have identified the Chl molecules involved in TTET to the central luteins in trimeric LHC-II by spectral simulation. These sites are, with the utmost probability, Chl603 and Chl612. The His and Asn residues, coordinating the central Mg atom of Chl603 and Chl612, respectively, pull the porphyrin ring toward the luteins, thus favoring the overlap of the conjugated systems. On the basis of the calculations and of the analysis of the EPR spectra, we cannot exclude that also Chl602 and Chl610 are involved, but this requires "ad hoc" changes of the ZFS axes directions of the luteins and specific ^{T}Chl spin sublevel populations.

We think that, in view of our results, the possibility that Chl603 and Chl612 might represent the red-most chlorophylls in the L2 and L1 domains should be reconsidered positively.

The formation of charge transfer states $Chl^{-}Car^{+}$ in LHC-II is prevented by the presence of a nonpolar environment, while the stringent structural requirements (close vicinity of the donor and acceptor) for efficient TTET are still fulfilled.

Unquenched triplet states of Chl molecules are present in the LHC-II complex. Putative sites of these triplet states are Chl614, Chl611, Chla604, and Chl613 since they do not contribute to the formation of the observed carotenoid triplet states.

Abbreviations

Car, carotenoid; Chl, chlorophyll; Lut, lutein; Nex, neoxanthin; Xat, xanthophyll; ZFS, zero field splitting; ISC, intersystem crossing; ESE, electron spin echo; FSE, field-swept echo; TR-EPR, time-resolved electron paramagnetic resonance; TTET, triplet−triplet energy transfer.

Acknowledgment. This work was supported by the Italian Ministry for University and Research (MURST) under the project PRIN2007. We thank Anna Segalla for kindly preparing the LHCII samples. Molecular graphics image (Figure 1) was produced using the UCSF Chimera package from the Resource for Biocomputing, Visualization, and Informatics at the University of California, San Francisco (supported by NIH P41 RR-01081).[44]

Supporting Information Available: A figure showing the TR-EPR spectrum of ^{T}Chl a in micelles of Triton X-100 and its simulation. A short description of the method used for TTET calculations and two figures showing the calculations of the spin polarization of ^{T}Car populated starting from the ^{T}Chl a population pattern *eaeaea*. Two figures showing the effect of rotation of the ^{T}Car ZFS axes around each of those initially determined by principal component analysis. This material is available free of charge via the Internet at http://pubs.acs.org.

References and Notes

(1) Liu, Z.; Yan, H.; Wang, K.; Kuang, T.; Zhang, J.; Gui, L.; An, X.; Chang, W. *Nature* **2004**, *428*, 287–292.

(2) Standfuss, J.; Terwisscha van Scheltinga, A. C.; Lamborghini, M.; Kuehlbrandt, W. *EMBO J.* **2005**, *24*, 919–928.
(3) Demmig-Adams, B.; Adams, W. W. *Trends Plant Sci.* **1996**, *1*, 21–26.
(4) Ruban, A. V.; Lee, P. J.; Wentworth, M.; Young, A. J.; Horton, P. *J. Biol. Chem.* **1999**, *274*, 10458–10465.
(5) Caffarri, S.; Croce, R.; Breton, J.; Bassi, R. *J. Biol. Chem.* **2001**, *276*, 35924–35933.
(6) Yan, H. C.; Zhang, P. F.; Wang, C; Liu, Z. F.; Chang, W. R. *Biochem. Biophys. Res. Commun.* **2007**, *355*, 457–463.
(7) Ruban, A. V.; Berera, R.; Ilioaia, C.; van Stokkum, I. H. M.; Kennis, J. T. M.; Pascal, A. A.; van Amerongen, H.; Robert, B.; Horton, P.; van Grondelle, R. *Nature* **2007**, *450*, 575.
(8) Moya, I.; Silvestri, M.; Vallon, O.; Cinque, G.; Bassi, R. *Biochemistry* **2001**, *40*, 2552–12561.
(9) Pascal, A. A.; Liu, Z. F.; Broess, K.; van Oort, B.; van Amerongen, H.; Wang, C.; Horton, P.; Robert, B.; Chang, W. R.; Ruban, A. *Nature* **2005**, *436*, 134–137.
(10) Barros, T.; Royant, A.; Standfuss, J.; Dreuw, A.; Kuhlbrandt, W. *EMBO J.* **2009**, *28*, 298–306.
(11) Holt, N. E.; Zigmantas, D.; Valkunas, L.; Li, X. P.; Niyogi, K. K.; Fleming, G. R. *Science* **2005**, *307*, 433–436.
(12) Avenson, T. J.; Ahn, T. K.; Zigmantas, D.; Niyogi, K. K.; Li, Z.; Ballottari, M.; Bassi, R. *J. Biol. Chem.* **2008**, *283*, 3550–3558.
(13) Frank, H. A.; Cogdell, R. J. *Photochem. Photobiol.* **1996**, *63*, 257–264.
(14) Carbonera, D.; Giacometti, G.; Agostini, G.; Toffoletti, A. *Gazz. Chim. Ital.* **1989**, *119*, 225–228.
(15) Carbonera, D.; Di Valentin, M.; Agostini, G.; Giacometti, G.; Liddel, P. A.; Gust, D.; Moore, A. L.; Moore, T. A. *Appl. Magn. Reson.* **1997**, *13*, 487–504.
(16) van der Vos, R.; Carbonera, D.; Hoff, A. J. *Appl. Magn. Reson.* **1991**, *2*, 179–202.
(17) Carbonera, D.; Giacometti, G.; Agostini, G. *Appl. Magn. Reson.* **1992**, *3*, 859–872.
(18) van der Vos, R.; Franken, E. M.; Hoff, A. J. *Biochim. Biophys. Acta* **1994**, *1188*, 243–250.
(19) Barzda, V.; Peterman, E. J. G.; van Grondelle, R.; van Amerongen, H. *Biochemistry* **1998**, *37*, 546–551.
(20) Lampoura, S. S.; Barzda, V.; Owen, G. M.; Hoff, A. J.; van Amerongen, H. *Biochemistry* **2002**, *41*, 9139–9144.
(21) Naqvi, K. R.; Melo, T. B.; Raju, B. B.; Javorfi, T.; Simidjiev, I.; Garab, G. *Spectrochim. Acta A* **1997**, *53*, 2659–2667.
(22) Peterman, E. J. G.; Dukker, F. M.; van Grondelle, R.; van Amerongen, H. *Biophys. J.* **1995**, *69*, 2670–2678.
(23) Mozzo, M.; Dall'Osto, L.; Hienerwadel, R.; Bassi, R.; Croce, R. *J. Biol. Chem.* **2008**, *283*, 6184–6192.
(24) Di Valentin, M.; Ceola, S.; Salvadori, E.; Agostini, G.; Carbonera, D. *Biochim. Biophys. Acta* **2008**, *1777*, 186–195.
(25) El-Sayed, M. A.; Tinti, D. E.; Yee, E. M. *J. Chem. Phys.* **1969**, *51*, 5721–5723.
(26) Ghanotakis, D. F.; Demetriou, D. M.; Yocum, C. F. *Biochim. Biophys. Acta* **1987**, *891*, 15–20.
(27) Akiyama, K.; Terokubota, S.; Ikoma, T.; Ikegami, Y. *J. Am. Chem. Soc.* **1994**, *116*, 5324–5327.
(28) Stoll, S.; Schweiger, A. *J. Magn. Reson.* **2006**, *178*, 42–55.
(29) Clarke, R. H. *Triplet State ODMR Spectroscopy. Techniques and Applications to Biophysical Systems*; Clarke, R. H., Ed.; Wiley-Interscience: New York, 1982.
(30) Di Valentin, M.; Ceola, S.; Agostini, G.; Giacometti, G. M.; Angerhofer, A.; Crescenzi, O.; Barone, V.; Carbonera, D. *Biochim. Biophys. Acta* **2008**, *1777*, 295–307.
(31) Kay, C. W. M.; Elger, G.; Mobius, K. *Phys. Chem. Chem. Phys.* **1999**, *1*, 3999–4002.
(32) Bittl, R.; Schlodder, E.; Geisenheimer, I.; Lubitz, W.; Cogdell, R. J. *J. Phys. Chem. B* **2001**, *105*, 5525–5535.
(33) Thurnauer, M. C. *Rev. Chem. Intermed.* **1979**, *3*, 197–230.
(34) Clarke, R. H.; Hotchandani, S.; Jagannathan, S. P.; Leblanc, R. M. *Chem. Phys. Lett.* **1982**, *89*, 37–40.
(35) Vrieze, J.; Hoff, A. J. *Chem. Phys. Lett.* **1995**, *237*, 493–501.
(36) Lendzian, F.; Bittl, R.; Telfer, A.; Lubitz, W. *Biochim. Biophys. Acta* **2003**, *1605*, 35–46.
(37) Frick, J.; Von Schutz, J. U.; Wolf, H. C.; Kothe, G. *Mol. Cryst. Liq. Cryst.* **1990**, *183*, 269–272.
(38) Hore, P. J. Analysis of Polarized EPR Spectra. In *Advanced EPR*; Hoff, A. J., Ed.; Elsevier Science Publishers B.V.: Amsterdam, 1989; pp 405−440.
(39) Closs, G. L.; Johnson, M. D.; Miller, J. R.; Piotrowiak, P. *J. Am. Chem. Soc.* **1989**, *11*, 3751–3753.
(40) Closs, G. L.; Piotrowiak, P.; MacInnis, J. M.; Fleming, G. R. *J. Am. Chem. Soc.* **1988**, *110*, 2652–2653.
(41) Berera, R.; Herrero, C.; van Stokkum, I. H. M.; Vengris, M.; Kodis, G.; Palacios, R. E.; van Amerongen, H.; van Grondelle, R.; Gust, D.; Moore, T. A.; Moore, A. L.; Kennis, J. T. M. *Proc. Natl. Acad. Sci. U.S.A.* **2006**, *103*, 5343–5348.
(42) Liddell, P. A.; Barrett, D.; Makings, L. R.; Pessiki, P. J.; Gust, D.; Moore, T. A. *J. Am. Chem. Soc.* **1986**, *108*, 5350–5352.
(43) Novoderezhkin, V. I.; Palacios, M. A.; van Amerongen, H.; van Grondelle, R. *J. Phys. Chem. B* **2005**, *109*, 10493–10504.
(44) Pettersen, E. F.; Goddard, T. D.; Huang, C. C.; Couch, G. S.; Greenblatt, D. M.; Meng, E. C.; Ferrin, T. E. *J. Comput. Chem.* **2004**, *25*, 1605–1612.

JP904012J